NANO LETTERS

2007
Vol. 7, No. 7
2089−2093

Nanoscale Mapping of Strain and Composition in Quantum Dots Using Kelvin Probe Force Microscopy

S. Shusterman,[†] A. Raizman,[†] A. Sher,[†] Y. Paltiel,*[,†] A. Schwarzman,[‡] E. Lepkifker,[‡] and Y. Rosenwaks*[,‡]

Solid State Physics, Electro-Optics Division, Soreq NRC, Yavne 81800 Israel, and School of Electrical Engineering—Physical Electronics, Faculty of Engineering, Tel-Aviv University, Tel-Aviv 69978, Israel

Received May 2, 2007; Revised Manuscript Received June 4, 2007

ABSTRACT

A key factor in improving quantum dots electrical properties and dots-based devices is the ability to control the crucial parameters of composition, doping, size, and strain distribution of the dots. We show that nanometer-scale work function measurements using ultrahigh vacuum Kelvin probe force microscopy is capable of measuring the strain and composition variations within and around individual QDs. This is accomplished by analyzing the detailed surface potential profiles in and around InSb/GaAs dots.

Nanometer-scale self-assembled dots in semiconductors are drawing a great deal of attention due to their unique atomlike quantum behavior.[1,2] The last two decades have witnessed tremendous progress in the ability to grow, synthesize, and fabricate high-quality semiconductor quantum dots (QDs) and QDs-based devices by a variety of techniques, and their basic structural, electrical, and optical properties were characterized by many authors.[3−6] In contrast to bulk or to quantum wells, in an ideal QD, the intersubband relaxation rate is small and may even exhibit a "phonon bottleneck" under weak excitation conditions.[7−9] In addition, dots can absorb normal incidence light in contrast to n-type quantum wells.[10] Thus, theoretically, the QDs confined in all three dimensions should have better optical properties than other quantum nanostructures.

However, many QD-based devices, for example light detectors, have not shown improved performance over simple quantum well detectors;[4] the main reasons are the inability to control the crucial parameters of composition, uniform doping, size, and strain distribution in the QDs, as well as the crystalline structure at the QDs−substrate interface and surfactant layers.[11] These factors reduce the confinement, the dot−substrate potential barriers, and introduce impurity levels in the energy gap.[12] Any attempt to improve the growth processes and the devices performance would benefit from quantitative measurements of strain distribution and composition variations in and around the individual dots. In this work, we show that nanometer-scale work function measurements using ultrahigh vacuum Kelvin probe force microscopy (UHV KPFM) is capable of measuring the strain and composition variations within and around individual QDs.

During the past decade, self-assembly of quantum dots has been observed in a wide variety of semiconductor systems.[3] Several methods for self-organized dots have been proposed, the most common among them is the Stranski−Krastanov (S−K) growth mode.[13] In this method, the deposited film is initially two-dimensional and then begins to form clusters on top of a wetting layer after 1−3 monolayers of growth. The S−K growth mode requires a large mismatch between the substrate and the QD material,[13,14] and this mismatch is one of the main driving forces leading to formation of the nanostructures, which are consequently highly strained.

Recently, an alternative approach to the QDs growth, known as the droplet heteroepitaxy (DHE) method,[15−17] has emerged. The DHE method consists of two basic stages: formation of group III element nanodroplets on the substrate and subsequent exposure of these droplets to the gas-phase flow of one or more group V elements. The method is very sensitive to the growth parameters but gives great flexibility in realizing QDs growth on different substrates. This method enables to grow narrow gap semiconductor QDs such as InSb or InAs on several types of substrates for potential use in optoelectronic devices active in the mid-IR wavelength region. Because no wetting layer is required in this growth

* Corresponding authors: paltiel@soreq.gov.il (Y.P.); yossir@eng.tau.ac.il (Y.R.).
[†] Soreq NRC.
[‡] Tel-Aviv University.

10.1021/nl071031w CCC: $37.00
Published on Web 06/23/2007

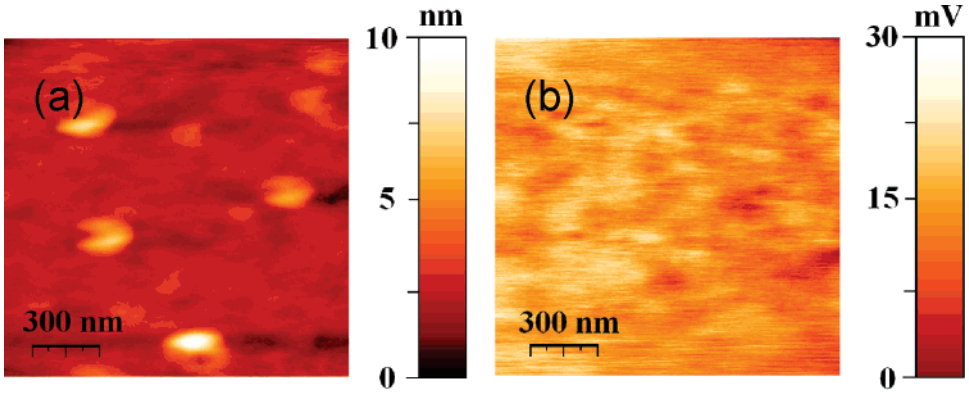

Figure 1. UHV KPFM measurements of InSb nanocrystals grown on InSb substrate. The 6 nm high dots are clearly observed in the topography image (a) and cannot be resolved in the CPD image (b).

mode, the strain can be controlled by using different substrates and variation of the growing conditions.[18]

Here we have used the DHE method for growing InSb nanostructures on n-type GaAs highly doped with Te, InSb, and GaSb (100) oriented substrates. The QD growth was carried out in a vertical reactor MOVPE machine (Thomas Swan Inc.) and was described in detail elsewhere.[18] The dots were grown using the same conditions on three different substrates; each dots−substrate system has different strain and electron affinity differences. In all cases, the dot size was in the range of 20−250 nm, and individual dots were well resolved in the topography atomic force microscope (AFM) images.

Our UHV KPFM measurements are based on a modified UHV AFM (VT AFM, Omicron Inc.)[19,20] operated at pressure $\leq 10^{-10}$ mbar. The topography was measured in the noncontact frequency modulation mode at the first cantilever resonance, while the ac voltage applied to the tip for the KPFM measurements was tuned to the second resonance frequency of the cantilever. This has enabled us to decrease the ac voltage applied to the tip to 50−150 mV and to avoid the tip-induced band bending effect as demonstrated by us recently.[21] The UHV KPFM has already been demonstrated as a powerful tool for measuring the work function variation over various quantum structures with nanometer resolution.[22−28]

Figure 1 shows UHV KPFM measurements of InSb dots grown on InSb substrate; the QDs are clearly observed in the topography image (a), but cannot be resolved in the CPD image (b). For convenience, the CPD is defined in this work as CPD $= (\phi_{tip} - \phi_{sample})/q$, where ϕ_{tip} and ϕ_{sample} are the work functions of the tip and the sample, respectively, and q is the elementary charge; therefore, a larger CPD means a smaller sample work function. As no strain and composition changes are induced in this system, no work function difference between the dots and the substrate is measured. In addition, the relatively large dots are uncapped; therefore, quantum confinement is expected only at low temperatures. The featureless KPFM images indicate that the islands curvature contribution to the work function variation due to a possible change in the surface energy is negligible.

Figure 2 presents UHV KPFM measurements of InSb nanocrystals grown on GaSb substrate. The actual dots size is 100−200 nm (Figure 2a); therefore, it is reasonable to assume that they are partially relaxed due to plastic deformation, and the work function variations are determined mainly by the composition changes. Figure 2c shows a CPD difference of 100−120 mV between the dot and the GaSb substrate that match the calculated value, obtained by taking into account the electron affinity,[29] band gap,[30] and valence band offsets[31] reported for these unstrained materials and summarized in Table 1.

Figure 3 shows topography (a) and CPD (b) images of 40 nm InSb nanodots, grown on n-doped GaAs. As in the InSb/GaSb system, a clear correlation between the two images is observed. However, the dark rings around the dots observed in the CPD image and the CPD peak heights do not match the work function difference between InSb and GaAs, expected only due to the composition changes. The same circular distribution of potential around S−K grown InAs dots on GaAs substrate was observed by Ono and Takahashi.[27,28] Figure 3c shows topography (solid line) and CPD (open circles) profiles along the green line in the two 2D images (a) and (b). The CPD profiles of the dots are narrower than the topography profiles, and two dips on both sides of the CPD peaks correspond to the circular depressions around the dots. An additional CPD peaks on each side outside the dot area is also measured by the KPFM; this is explained in detail below by taking into account the strain and the composition changes.

Figure 4 shows high-resolution TEM images of InSb dots grown on GaAs and capped with a 70 nm thick GaAs layer. The capped dots and their vicinity have different lattice parameters and are thus strained. Figure 4a shows a typical HRTEM image of the structure in the vicinity of a QD; the dots have a crystalline structure and the same orientation as the substrate, which means that the DHE dots grow epitaxially in the [110] direction. Figure 4b shows the fast Fourier transform (FFT) of the following areas: (1) GaAs substrate, (2) QD, and (3) GaAs cap layer; it should be noted that the dot size is half of the FFT averaged area. Lattice parameters were calculated from the FFT measurements: 5.74 ± 0.02 Å for the GaAs substrate, 6.06 ± 0.03 Å for the nanodot, and 5.73 ± 0.04 Å for the GaAs cap layer. The lattice parameter obtained for the QD is smaller than the bulk lattice parameter of pure InSb (6.47 Å), indicating that the dots grown by DHE on GaAs have a composition of $InAs_{1-x}Sb_x$ rather than pure InSb. According to our estimation, the dots contain approximately 20% of Sb.[18] Figure 4c shows the

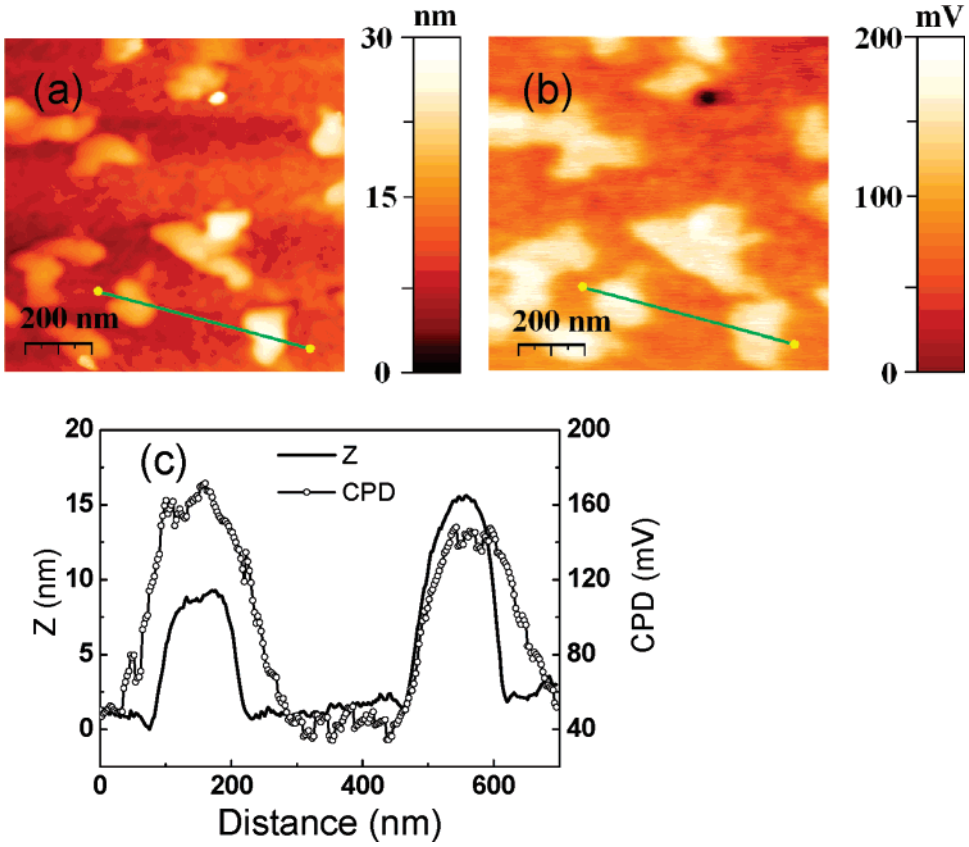

Figure 2. UHV topography (a) and KPFM measurements (b) of InSb nanocrystals grown on GaSb substrate. (c) topography (solid line) and CPD (open circles) profiles along the green lines on images (a) and (b). The measured 100−120 mV work function difference between the GaSb clusters and the InSb substrate is due to the different electron affinity, band gap, and valence band offset between the two materials.

Table 1. Electron Affinity and Band Structures Parameters of the Relevant Materials Used Our Calculations

	a_o (Å)	E_g 300 K (eV)	C_{11} (10^9 dyn/cm^2)	C_{12} (10^9 dyn/cm^2)	a_c (eV)	$\Delta E_V = E_V - E_{VInSb}$ (eV)	χ (eV)
InSb	6.479	0.18	660	360	−6.17	0	4.59
GaSb	6.095	0.72	880	400	−6.85	0.08	4.06
InAs	6.058	0.35	830	450	−5.08	−0.43	4.90
GaAs	5.653	1. 43	1121	566	−7.17	−0.60	4.07

bright-field cross-section TEM image of two dots layers and strain-produced defects in the GaAs substrate and cap layers. The dashed lines at the boundaries of the dark areas below (substrate) and above (cap layer) the QD represent strained regions.

Several factors may affect the work function variation across the QDs: dots composition inhomogeneity due to interdiffusion or dissolving of the substrate material by liquid In droplet,[18] mismatch strain presented in both the substrate and the dots,[12,32] doping level variation,[21] strain-dependent piezoelectric band shifts,[33] surface states,[21,24] quantum effects,[25] and 2D electron gas formation. In the analysis below, we assume that, at room temperature, due to small dimensions of the dots and the high substrate doping, only the first three factors determine the QDs work function variations.

The KPFM measurements were carried out on uncapped dots, which are less strained, as the stress is only due to the substrate. Assuming that the capped and uncapped dots have the same composition, a good estimation of the expected work function variation in the InSb QDs/GaAs can be obtained. Figure 4 shows that As, diffusing from the GaAs substrate, penetrates the dots; therefore, for a large enough uncapped dot, there is a gradual composition change from the As-rich $InAs_xSb_{1-x}$ region in the bottom of the dot to the Sb-rich $InAs_xSb_{1-x}$ at the top of the dot. The estimated work function difference between the two materials is 50 meV;[29−31] in such a case, we expect a gradual decrease of the CPD profile toward the center of the dot. However, the fact that the measured CPD profile in Figure 3c wiggles indicates that the composition change alone cannot account for such work function changes, as we show in detail below.

While quantum well layers are subjected to a homogeneous strain and have well-defined band edges, quantum dots with volume smaller than some critical value undergo an elastic strain relaxation, which strongly depends on the local thickness of the deposited material. The strain distribution in coherent uncapped dots was calculated numerically by Spencer and Tersoff[12] and Johnson and Freund.[34] The dot

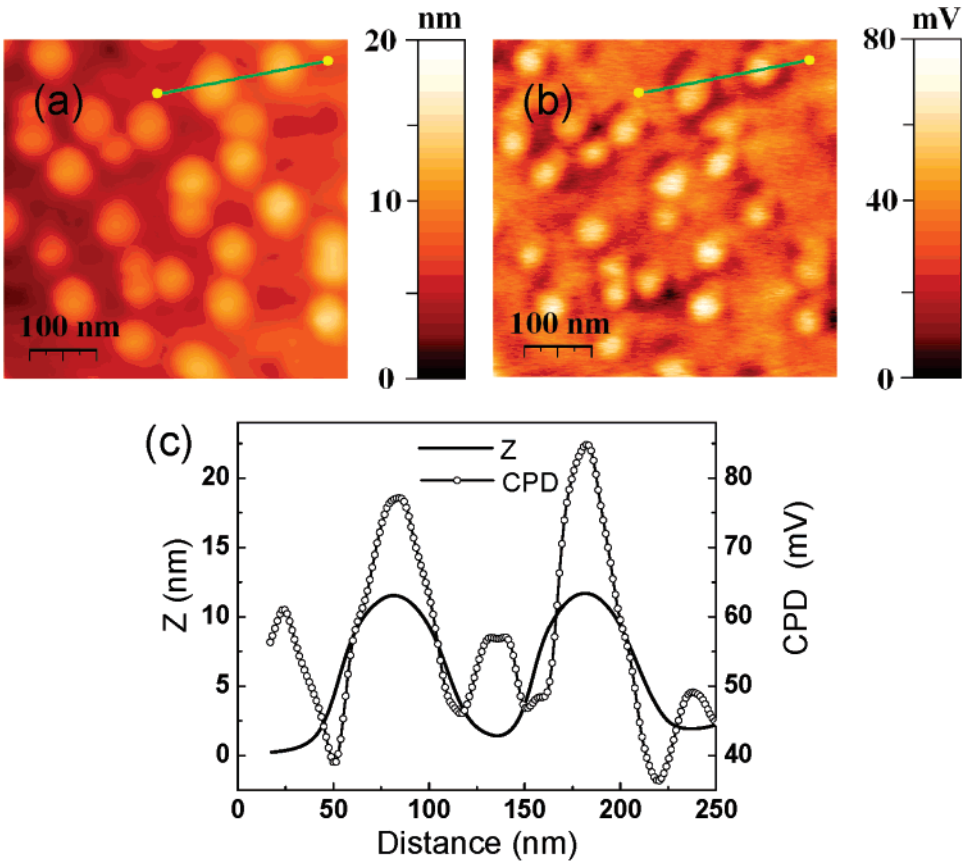

Figure 3. UHV topography (a) and KPFM measurements (b) of InSb nanodots grown on GaAs substrate, (c) topography (solid line) and the CPD or surface potential (open circles) profiles along the green lines on images (a) and (b). The typical CPD profile of single QD consist of a sharp deep, surrounded by a higher region.

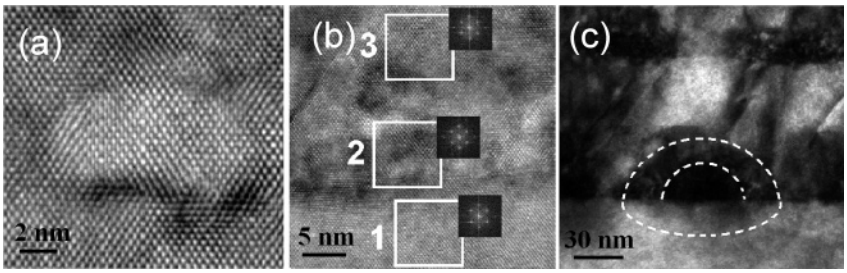

Figure 4. High-resolution TEM images of InSb dots grown on GaAs. (a) Atomic structure in the vicinity of single QD. The semispherical dots are crystalline, defect free, and coherent with the substrate and the cap layer. (b) Few layers of substrate dot and cap. The insets show fast Fourier transform (FFT) of: (1) GaAs substrate, (2) QD, (3) GaAs cap layer. Lattice parameters were calculated from the FFT measurements and found to be at 5.74 ± 0.02 Å for the GaAs substrate, 6.06 ± 0.03 Å for the nano dot, and 5.73 ± 0.04 Å for the GaAs cap layer. The lattice parameter of dot indicates that the dot's average composition is $InAs_{1-x}Sb_x$ rather than pure InSb. (c) Bright-field cross-sectional TEM image of few layers of the InSb QDs grown on GaAs substrate with 70 nm GaAs cap layers. The dashed lines represent strained regions below (in substrate) and above (in cap layer).

edges are exposed to the largest strain, which decreases to zero toward the dots center due to elastic relaxation. The GaAs substrate is subjected to a compressive strain in the vicinity of the dot edge, and this strain partially compensates the tensile strain exerted on it by the dot; far from the dot, the substrate is fully relaxed. The measured CPD depends on the conduction band minimum energy, E_C, which change with the strain as $\Delta E_C = a_c(2\epsilon_{||} + \epsilon_\perp)$; here a_c is the conduction band hydrostatic deformation potential constant, and $\epsilon_{||}$ and $\epsilon_\perp$ are the lateral and vertical mismatch strains, respectively. The relation between $\epsilon_{||}$ and $\epsilon_\perp$ is given by $\epsilon_\perp = -(2C_{12}/C_{11})\cdot\epsilon_{||}$, where C_{11} and C_{12} are the elastic constants of the material. Because $a_c < 0$, compressive and tensile strains yield positive and negative E_C and CPD changes, respectively.

Figure 5a shows the calculated CPD variations caused by the composition changes (dashed), by the near-surface strain contributions (dotted), and by a superposition of these two factors (solid line). Our two-dimensional model assumes a linear elastic behavior, with smooth cosine-like variations of the composition and strain profiles for both the substrate and the dots. The dot size was approximated as 10 nm in height and with a base diameter of 40 nm. Because of the small height of the dots, only elastic relaxation was consid-

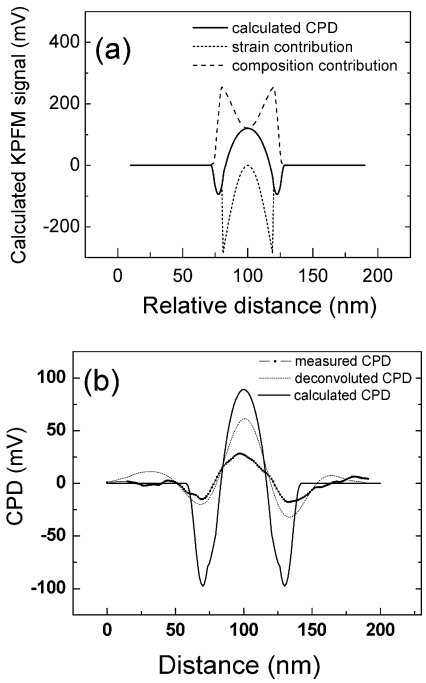

Figure 5. Estimated CPD signal variations. (a) Composition changes composed of affinity and conductive band edge changes (dashed line) are not sufficient to explain the CPD results. Adding the calculated strain contribution (doted line) yields a curve (solid line) that clearly resembles measured CPD results of InSb QD on GaAs. (b) The assumed measured results (black square line), calculated CPD profile (solid line), and deconvoluted (doted line) results. Note the great similarity to Figure 3 experimental results. The zero baseline in both figures is attributed to the calculated local vacuum level of GaAs (−4.89 V). It seems that strain and composition changes are the main contributors to the CPD profile.

ered, and the top of the QD was assumed to be fully elastically relaxed and the edges fully strained.[34] The lattice constants were taken from the HR TEM measurements; electron affinity and band structure parameters of the relevant materials were taken from reported data[12,29−31] and are summarized in Table 1. We have also assumed that the dots composition changes gradually from InAs to InSb, resulting in a smooth change in the band gap and electron affinity.

Figure 5b shows the calculated CPD profile (solid line) in comparison with the measured CPD (large dots) and the restored (small dots) CPD profile of one of the dots in Figure 3b. The restoration of CPD images, described by us in detail recently,[35] is based on deconvolution of the measured image with a calculated tip point spread function by taking into account the experimental noise. We did not attempt to match exactly the restored CPD profile because we anticipate that additional factors (apart from the strain and composition considered here) may contribute to the CPD variation. Nevertheless, we argue that, because these two factors have the largest effect on the measured surface potential, the KPFM can become an important tool for in situ composition and strain measurements in and around individual QDs.

In summary, we have used ultrahigh vacuum Kelvin probe force microscopy to extract the strain and composition variations in and around epitaxially grown QDs. We anticipate that this method, which can be used in situ, will lead to a better control of dots composition, uniform doping, size, and strain distribution, as well as the crystalline structure at the QDs−substrate interface. Understanding and optimization of these crucial parameters will have a large impact on dots growth in general, and on their integration in devices in particular.

References

(1) Kazarinov, R. F.; Suris, R. A. *Sov. Phys. Semicond.* **1971**, *5*, 797.
(2) Turton, R. *The Quantum Dot: A Journey into Future Microelectronics*; Oxford University Press: New York, 1996.
(3) Borovitskaya, E.; Shur, M. S. *Quantum Dots, Selective Topics in Electronics and Systems*; World Scientific Publishing: Singapore, 2002.
(4) Krishna, S.; Stiff-Roberts, A. D.; Phillips, J. D.; Bhattacharya, P.; Kennerly, S. W. *IEEE Circuits Devices Mag.* **2002**, *1*, 14.
(5) Shchekin, O. B.; Deppe, D. G. *Appl. Phys. Lett.* **2002**, *80*, 3277.
(6) Ledentsov, N. N.; Bimberg, D.; Ustinov, V. M.; Alferov, Z. I.; Lott, J. A. *Physica E* **2002**, *13*, 871.
(7) Sumpf, B.; Deubert, S.; Erbert, G.; Fricke, J.; Reithmaier, J. P.; Forchel, A.; Stske, R.; Tränkle, G. *Electron. Lett.* **2003**, *39*, 23.
(8) Alivisatos, A. P. *Science* **1996**, *271*, 933.
(9) Heitz, R.; Born, H.; Guffarth, F.; Schliwa, O.; Hoffmann, A.; Bimberg, D. *Phys. Rev. B*, **2001**, *64*, 241305(R).
(10) Heitmann, D.; Kotthaus, J. P. *Phys. Today* **1993**, *46*, 56.
(11) Lim, H.; Zhang, W.; Tsao, S.; Sills, T.; Szafraniec, J.; Mi, K.; Movaghar, B.; Razeghi, M. *Phys. Rev. B* **2005**, *72*, 085332.
(12) Pryor, C. E.; Pistol, M.-E. *Phys. Rev. B* **2005**, *72*, 205311.
(13) Eaglesham, D. J.; Cerullo, M. *Phys. Rev. Lett.* **1990**, *64*, 1943.
(14) Mo, Y.-W.; Sawage, D. E.; Swartzentruber, B. S.; Lagally, M. G. *Phys. Rev. Lett.* **1990**, *65*, 1020.
(15) Lee, C.-D.; Park, C.; Lee, H. J.; Park, S. J.; Lee, K.-S.; Park, C. G.; Noh, S. K. *J. Surf. Anal.* **1998**, *4*, 299.
(16) Mano, T.; Watanabe, K.; Tsukamoto, Sh.; Fujioka, H.; Oshima, M.; Koguchi, N. *Jpn. J. Appl. Phys.* **1999**, *38*, 1009.
(17) Ro, J.-R.; Kim, S.-B.; Park, K.; Lee, E.-H.; Lee, J. *J. Cryst. Growth* **1999**, *201/202*, 1198.
(18) Shusterman, S.; Paltiel, Y.; Sher, A.; Ezersky, V.; Rosenwaks, Y. *J. Cryst. Growth* **2006**, *291*, 363.
(19) Kikukawa, H. A.; Hosaka, S.; Imura, R. *Rev. Sci. Instrum.* **1996**, *67*, 1463.
(20) Sommerhalter, Ch.; Matthes, Th. W.; Glatzel, Th.; Jaeger-Waldau, A.; Lux-Steiner, M.Ch. *Appl. Phys. Lett.* **1999**, *75*, 286.
(21) Rosenwaks, Y.; Shikler, R.; Glatzel, Th.; Sadewasser, S. *Phys. Rev. B* **2004**, *70*, 085320.
(22) Nonenmacher, M.; O'Boyle, M. P.; Wickramasing, H. K. *Appl. Phys. Lett.* **1991**, *58*, 2921.
(23) Sadewasser, S.; Glatzel, Th.; Rusu, M.; Jäger-Waldau, A.; Lux-Steiner, Ch. M. *Appl. Phys. Let.* **2002**, *80*, 2979.
(24) Glatzel, Th.; Fuertes Marron, D.; Schedel-Niebdrig, Th.; Sadewasser, S.; Lux-Steiner, M. Ch. *Appl. Phys. Let.* **2002**, *81*, 2017.
(25) Yamauchi, T.; Tabuchi, M.; Nakamura, A. *Appl. Phys. Lett.* **2004**, *84*, 3834.
(26) Schwarzman, A.; Grunbaum, E.; Strassburg, E.; Lepkifker, E.; Boag, A.; Rosenwaks, Y.; Glatzel, Th.; Barkay, Z.; Mazzer, M.; Barnham, K. *J. Appl. Phys.* **2005**, *98*, 084310.
(27) Ono, S.; Takahashi, T. *Jpn. J. Appl. Phys.* **2005**, *44*, 6213.
(28) Ono, S.; Takahashi, T. *Jpn. J. Appl. Phys.* **2006**, *45*, 1931.
(29) Milnes, A. G.; Feucht, D. L. *Heterojunction and Metal−Semiconductor Junctions*; Academic Press: New York, 1972.
(30) Van Vechten, J. A. *Phys. Rev.* **1969**, *187*, 1007.
(31) Tsou, Y.; Ichii, A.; Garmire, E. M. *IEEE J. Quantum Electron.* **1992**, *28*, 1261.
(32) Spencer, B. J.; Tersoff, J. *Phys. Rev. B* **2001**, *63*, 205424.
(33) Pan, E. *J. Appl. Phys.* **2002**, *91* 6379.
(34) Johnson, H. T.; Freund, L. B. *J. Appl. Phys.* **1997**, *81*, 9.
(35) Strassburg, E.; Boag, A.; Rosenwaks, Y. *Rev. Sci. Instrum.* **2005**, *76*, 83705.

NL071031W